Journal of Palaeosciences 72(2023): 119–126
2583–4266/2023
https://doi.org/10.54991/jop.2023.1860

Late Oligocene atmospheric carbon dioxide concentrations reconstructed from fossil leaves using stomatal index

TEKIE F. TESFAMICHAEL

Addis Ababa University, College of Natural and Computational Sciences, Addis Ababa 1176, Ethiopia.
Email: tekie.fisseha@aau.edu.et

(Received 22 May, 2023; revised version accepted 30 November, 2023)

ABSTRACT

Tesfamichael TF 2023. Late Oligocene atmospheric carbon dioxide concentrations reconstructed from fossil leaves using stomatal index. Journal of Palaeosciences 72(2): 119–126.

Ancient atmospheric CO_2 can be reconstructed using various climate proxies; stomata from fossil leaves are one of the climate proxies that provide critical information about past climatic conditions of the Earth. Exceptionally well–preserved fossil leaves found in overbank deposits in Chilga of Northwest Ethiopia were used to estimate late Oligocene atmospheric CO_2 values using stomatal index. The age of the fossils, $^{206}Pb/^{238}U$: 27.23 ± 0.03 Ma, was determined from zircons in an ash deposit comprising the matrix deposited contemporaneously with the fossil leaves. Stomatal indices were calculated from both the fossil leaves and nearest living relatives of the fossils. Corresponding atmospheric CO_2 values for the nearest living relatives of the fossils were assigned from historical records from the Mauna Loa Observatory. This produces a calibrating curve that shows variation of atmospheric CO_2 overtime, and late Oligocene atmospheric CO_2 values were quantified from the calibrating curve. The quantified late Oligocene atmospheric CO_2 values are about 343 ± 11 ppm which show a 12 % decrease when they are quantified using a leaf gas exchange method. This is consistent with the idea that stomatal–index method underestimates CO_2 values compared to the leaf gas exchange method. The late Oligocene was colder than both its preceding Eocene and its following Miocene epochs, and the results are in congruent with the cold Oligocene Period. These results for this particular geologic time provide opportunity to examine how plants responded to climate changes in the past and have important implications for the study of current and future climate changes.

Key–words—Late Oligocene, atmospheric CO_2, Stomatal index, fossil leaves, Ethiopia.

INTRODUCTION

EARTH'S climate has varied from greenhouse climate to icehouse climate and vice versa over the geologic time period (Grein *et al*., 2013; Montañez & Poulsen, 2013; Tesfamichael *et al*., 2017; Hutchinson *et al*., 2020; Liu *et al*., 2021). The fluctuation of Earth's climate from greenhouse to icehouse climate and vice versa shows an overall climate variation pattern. However, the details of climatic variations for each geologic time interval have not been yet fully recognized. This is partly due to lack of climate proxies for each geologic time interval and lack of appropriate chemical elements used to constrain the age of proxies. An overbank deposit found in the Northwest Ethiopia of Chilga provides well–preserved fossil leaves with well constrained age, 27.23 ± 0.03 Ma (Tesfamichael *et al*., 2017) (Fig. 1). The age of the fossil leaves was determined using $^{206}Pb/^{238}U$ dating method from zircon minerals deposited contemporaneously with the fossil leaves. These fossil leaves provide opportunity to quantify late Oligocene atmospheric CO_2 concentrations. Atmospheric CO_2 values quantified from these proxies refine our understanding of earth's climate variations; and these CO_2 values also improve resolution of climate models as CO_2 values from proxies fill data gaps in climate modelling. Fig. 1 shows the locality from where the current late Oligocene fossil leaves are collected.

The Oligocene geologic time is characterized by the transformation of terrestrial phytocoenoses from primarily evergreen vegetation to mixed mesophytic forests (Utescher *et al*., 2020), and other tectonic and climatic changes (Hutchinson *et al*., 2020; Sun *et al*., 2021). Analysis of oxygen isotope composition from deep sea sediments shows an abrupt increase in $\delta^{18}O$ values implying a combination of an ice sheet growth, a cooling event, and a worldwide drop in sea level during the early Oligocene which affected the lives of several organisms (Zachos *et al*., 2008; Houben *et al*., 2012; Hutchinson *et al*., 2020; Vries *et al*., 2021). This period is marked by a mass extinction of marine organisms such as benthic foraminifera (Cotton & Pearson, 2011), and had major impact in mammal faunal communities in Europe (Escarguel *et al.*, 2008). The climate shift during the early Oligocene had also its impact in Africa; more than two–thirds of mammals in Africa and the Arabian Peninsula went extinct during this time (Vries *et al*., 2021). Floral distribution was also affected during the Oligocene; broad–leaved plants became confined to lower latitudes, and grasslands started to expand (Shockey & Anaya, 2011). In terms of tectonics, important opening and closing of ocean gateways such as Drake Passage and the Tethys seaway played a significant role in the Oligocene climate (Wang *et al*., 2020; Hodel *et al*., 2021). These tectonic activities reshaped the ocean circulation and in turn the climate (Sun *et al*., 2021); parts of Yemen were also connected to East Africa, and this land bridge between Africa and Asia facilitated migration of mammals between the two continents (Kappelman *et al*., 2003; Sen, 2013). All these major events made the Oligocene very significant period. Hence, obtaining and analyzing fossil leaf data from this time period has significant contribution towards developing scientific evidence for reconstructing paleoclimate and paleoenvironment of the time.

Stomatal densities from fossil leaves provide vital information about concentration of earth's atmospheric CO_2. The basis for the stomatal index method of estimating atmospheric CO_2 values from fossil leaves is the inverse relationship between stomatal densities and atmospheric CO_2 values which is demonstrated in a wide range of various plant taxa grown in various geological and ecological settings (Royer, 2001; Roth–Nebelsick, 2005; McElwain & Haworth, 2009; Steinthorsdottir & Vajda, 2015). Although this method is well established, lack of exquisitely preserved fossil leaves impedes reconstruction of ancient atmospheric CO_2. Here late Oligocene atmospheric CO_2 values are reconstructed from fossil leaves using stomatal index (Fig. 2). The quantified atmospheric CO_2 values offer an additional input to our understanding of the Oligocene climate and fill data gaps in climate modelling.

GEOLOGIC SETTING

The geological setting of Northwest Ethiopia where the Chilga locality lies is characterized by a succession of Oligocene–aged (30 Ma) flood basalts (Coulie *et al*., 2003; Kieffer *et al*., 2004) and felsic volcanic rocks. These flood basalts, some 2000 m thick, comprise the bulk of the Ethiopian Highlands stratigraphic succession and form the basal deposits in the Chilga sedimentary sequence, today at 1930 m. Some areas of the Ethiopian Highlands are overlain by Miocene and younger shield volcanoes and related basalts, and have interbedded fossiliferous sedimentary rocks, ranging in age from late Oligocene to Pleistocene (Ayalew *et al*., 2002; Kieffer *et al*., 2004). The fossil leaves come from overbank

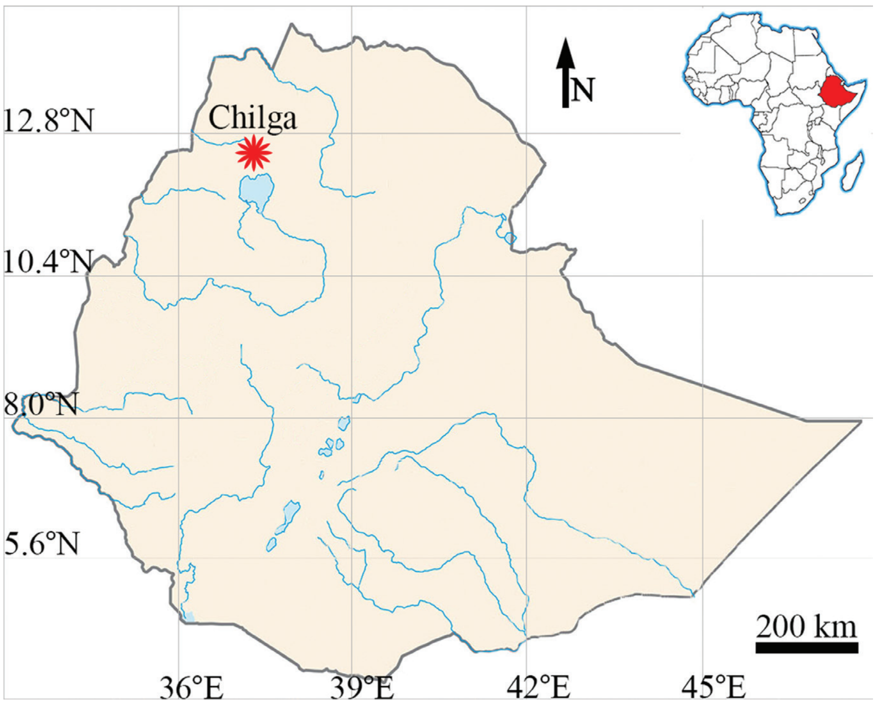

Fig. 1—Location map of the late Oligocene fossil leaves at Chilga.

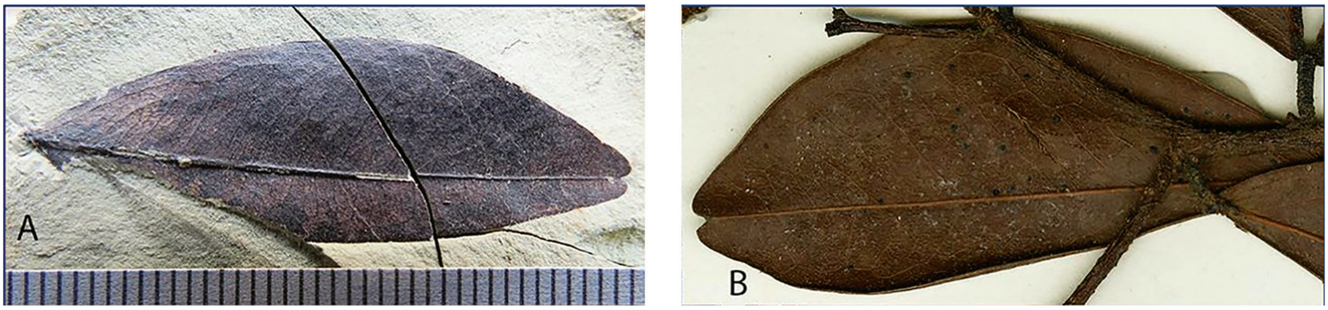

Fig. 2— (A) Fossil leaf of *Cynometra chaka* from Chilga. (B) One of the closest living relatives *Cynometra bauhiniafolia*.

deposits found in Northwest of Ethiopia, the Chilga area (Fig. 1). The age of the fossils is (27.23 ± 0.03 Ma) determined from zircons deposited contemporaneously with the plant fossils (Tesfamichael *et al*., 2017).

MATERIALS AND METHODS

The materials used to reconstruct late Oligocene atmospheric CO_2 values are fossil leaves of *Cynometra* sp. (Pan *et al*., 2010). The fossil leaves were collected from late Oligocene strata in Northwest Ethiopia at Chilga and were brought to the National Museum of Ethiopia for further laboratory analyses. Comparative analysis of the fossil leaf with its nearest living relative has been carried out by Aaron Pan (Pan *et al*., 2010) and the fossil leaf is taxonomically described and placed within the genus *Cynometra* (Pan *et al*., 2010). Following the works of Pan *et al*. (2010) on the fossil leaves, closely related living plant species to the fossil leaves has been collected from the genus *Cynometra* in order to estimate atmospheric CO_2 of the late Oligocene. The living relatives for the fossil leaves were obtained from herbarium collections of the Botanical Research Institute of Texas (BRIT), USA and Missouri Botanical Garden (MS), USA (Table 1).

In order to process cuticle images, small fragments of fossil leaves about 0.5 cm^2 were taken from the complete fossil leaves (Fig. 2A), and these fossil leaf specimens were immersed in 10% hydrochloric acid for about 30–50 minutes

Table 1—Stomatal index and corresponding CO_2 values used to produce a calibrating curve.

No.	Specimen # and herbarium leaves	Stomatal Index (%)	pCO_2 (ppm)	Year specimens collected
1	BRIT330729, *Cynometra kauhi*	17.15	327	1972
2	BRIT330728, *Cynometra bauhiniafolia*	22.04	327	1972
3	BRIT330725, *Cynometra spruceana*	19.94	345	1984
4	BRIT330726, *Cynometra retrusa*	14.47	349	1987
5	BRIT29170, *Cynometra mirabilis*	14.52	356	1991
6	BRIT29171, *Cynometra bauhiniafolia*	13.53	356	1991
7	BRIT29172, *Cynometra ramiflora*	15.51	356	1992
8	BRIT330727, *Cynometra retrusa*	17.66	356	1992
9	BRIT330723, *Cynometra* sp.	17.60	356	1992
10	BRIT330732, *Cynometra longicuspis*	17.12	363	1996
11	BRIT330731, *Cynometra affaurita*	16.03	364	1997
12	BRIT330730, *Cynometra webberi*	11.69	368	1999
13	MS5573357, *Cynometra lujae*	14.50	370	2000
14	MS5547517, *Cynometra lujae*	11.72	370	2000
15	MS5993731, *Cynometra lukei*	15.46	376	2003
16	MS6455795, *Cynometra lukei*	12.51	382	2006

to remove any carbonate materials from the matrix adhering to cuticles (Tesfamichael *et al*., 2017). After rinsing with distilled water, the specimens were placed in 48% hydrofluoric acid for 48 hours to remove silicate matrix from the cuticles. Then, cuticles were peeled off from the treated fossil leaves; next the cuticles were mounted on microscope slides and observed under an Epifluorescence Microscope. Finally, several cuticle images were taken using a high resolution digital camera attached to the Epifluorescence Microscope and with the help of Leica Application Suite software. The cuticles were magnified up to 400 times; as a result, stomata, epidermal cells, and micro leaf structures became clearly visible (Fig. 3). Three rectangular areas each about 0.15 mm^2 were delineated from each fossil leaf using ImageJ software (Version 127 1.48v, Rasband, 2016). Stomata and epidermal cells inside the rectangular areas and those that touch the boundary line of the rectangular area were counted; stomatal density and epidermal cell density for each area were determined by dividing the numbers of stomata and epidermal cells to the area of the rectangle. Once the stomatal density and epidermal cell density are calculated, stomatal index is quantified using the following equation (Equation 1).

$$\text{Stomatal Index}(\%) = \frac{\text{stomatal density}}{\text{stomatal density} + \text{epidermal cell density}} \text{X } 100 \; \ldots\ldots\ldots (1)$$

The nearest extant relatives to the fossil leaves were collected from herbarium collections at Missouri Botanical Garden (USA), and Botanical Research Institute of Texas (USA) based on comparisons of morphological and cuticular features, and small samples, 1cm by 1cm, were taken from each herbarium specimens, and stomata and epidermal cells are counted from the abaxial surfaces of 16 herbarium leaves (Table 1).

The preparation of cuticle images for the extant species required immersion in distilled water for two to three days to rehydrate the specimens. When the specimens are not rehydrated well, they are additionally treated with 10% potassium hydroxide (KOH) followed by a dilute solution of NaOCl (household bleach) (Tesfamichael *et al*., 2017). Finally images of cuticles with clearly visible stomata and epidermal cells were produced using a Leica DM2000 Epifluorescence Microscope and a high resolution digital camera attached to the microscope. From these, stomatal and epidermal cell counts were made using ImageJ Software (Version 127 1.48v, Rasband, 2016) which led to quantify stomatal indices of the nearest extant relatives of the fossil leaves (Table 1). Once stomatal indices of the herbarium leaves are determined, corresponding atmospheric CO_2 values for the closely related extant species to the fossils were assigned from historical records from the Mauna Loa Observatory (https://gml.noaa.gov/webdata/ccgg/trends/co_2/co_2_annmean_mlo.txt). This produces a calibrating curve that shows variation of atmospheric CO_2 overtime (Fig. 4), and the late Oligocene atmospheric CO_2 values are quantified using the calibrating curve (Table 2).

$$pCO_2 \text{ (paleo)} = 566.25^*(SI^{-0.168}) \quad \ldots\ldots\ldots\ldots \quad (2)$$

RESULTS

The results of stomatal indices of the living relatives for the fossil leaves are provided in Table 1 with the corresponding atmospheric CO_2 values. The stomatal indices and the corresponding atmospheric CO_2 values enable to produce the calibrating curve (Fig. 4). The calibrating curve is used to reconstruct the late Oligocene atmospheric CO_2. Table 2 shows concentration of atmospheric CO_2 for the late Oligocene. The results range from 325 ppm to 364 ppm with grand mean of 343 ± 11 ppm which indicate a 12% decrease when they are quantified using a leaf gas exchange method ($C_a = \frac{A_n}{g_{c(tot)}(1 - C_i/C_a)}$) that resulted in 390 ppm

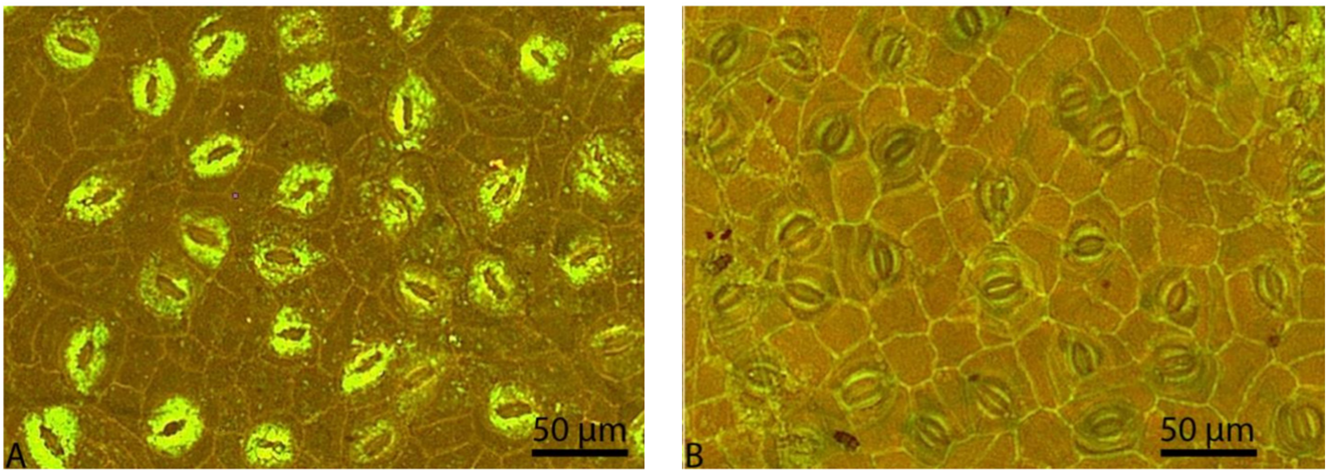

Fig. 3—(A) Stomata and Epidermal cells on cuticles of fossil leaf. (B) Corresponding extant leaf *Cynometra longicuspis*.

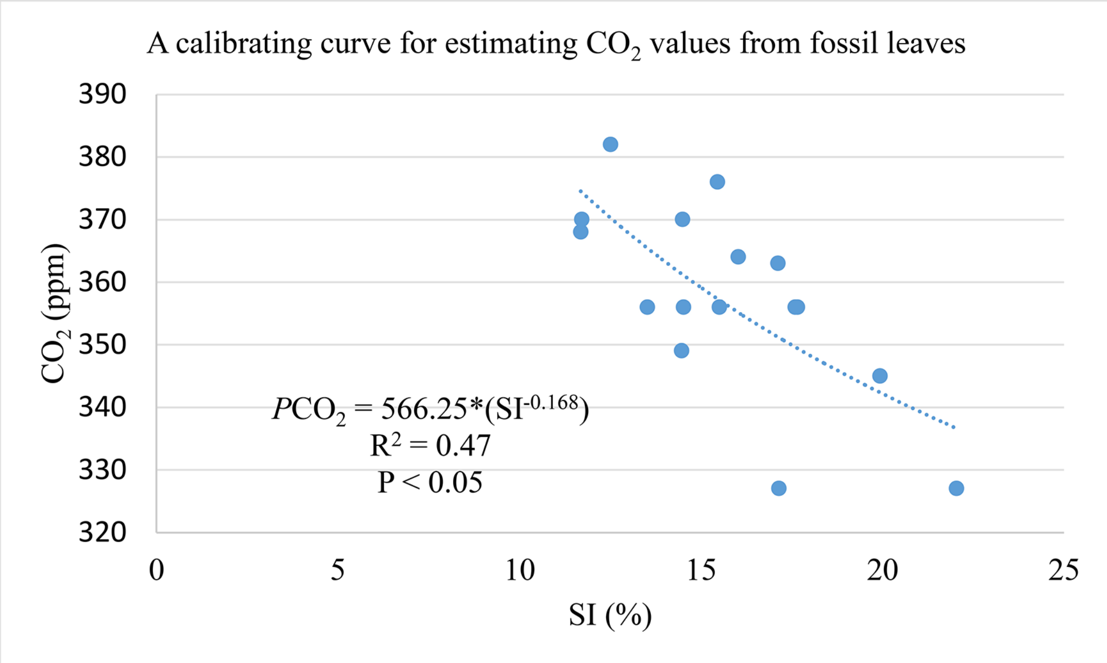

Fig. 4—Stomatal index (SI) of extant plants plotted against known atmospheric CO_2 used to calibrate fossil stomatal indices.

(Tesfamichael *et al*., 2017), where, C_a is atmospheric CO_2 concentration (in ppm); A_n is the net rate of CO_2 assimilation by leaves (in µmol m^{-2} s^{-1}); g_c is operational conductance to CO_2 diffusion from the atmosphere to sites of photosynthesis within the leaf (in mol m^{-2} s^{-1}); and C_i is CO_2 concentration inside the leaf (Franks *et al*., 2014).

This is consistent with idea that stomatal–index method underestimates CO_2 values compared the leaf gas exchange method (Konrad *et al*., 2021).

The calibrating curve (equation 2) is produced using the data collected from the living relatives of the fossil leaves (Table 1). The relationship between the concentration of atmospheric CO_2 and stomatal index was assessed for N = 16 herbarium leaves of *Cynometra* species. The quantified late Oligocene atmospheric CO_2 values are about 343 ± 11 ppm which are in congruent with the hypothesis that the late Oligocene was colder than both the preceding Eocene and the following Miocene epochs (O'Brien *et al*., 2020); hence, concentration of atmospheric CO_2 of the late Oligocene has contributed for the cold climate during the late Oligocene.

DISCUSSION AND CONCLUSION

The quantified late Oligocene atmospheric CO_2 values are about 343 ± 11 ppm which show a 12% decrease when they are quantified using a leaf gas exchange method that resulted in 390 ppm (Tesfamichael *et al*., 2017). This is consistent with the idea that stomatal–index method underestimates CO_2 values compared to the leaf gas exchange method (Konrad

Table 2—Late Oligocene atmospheric CO_2 derived from a calibrating curve from stomatal index.

Fossil Leaf Specimens	**Age (Ma)**	**Stomatal Index (%)**	**pCO_2 (ppm)**
CH40–P100(2)	27.23	19.76	343
CH40–P31	27.23	22.56	335
CH–40–125A	27.23	25.79	328
CH41–67	27.23	23.89	332
CH40–P100(1)	27.23	17.85	349
CH40–169	27.23	20.15	342
CH40–173A	27.23	19.76	343
CH41–70	27.23	27.19	325
CH40–P70	27.23	14.94	360
CH52–98A	27.23	23.98	332
CH41–13	27.23	19.51	344
CH40–P95(2)	27.23	17.87	349
CH41–63	27.23	13.78	364
CH40–P49	27.23	16.58	353
Grand mean of pCO_2 (ppm)			**343 ± 11**

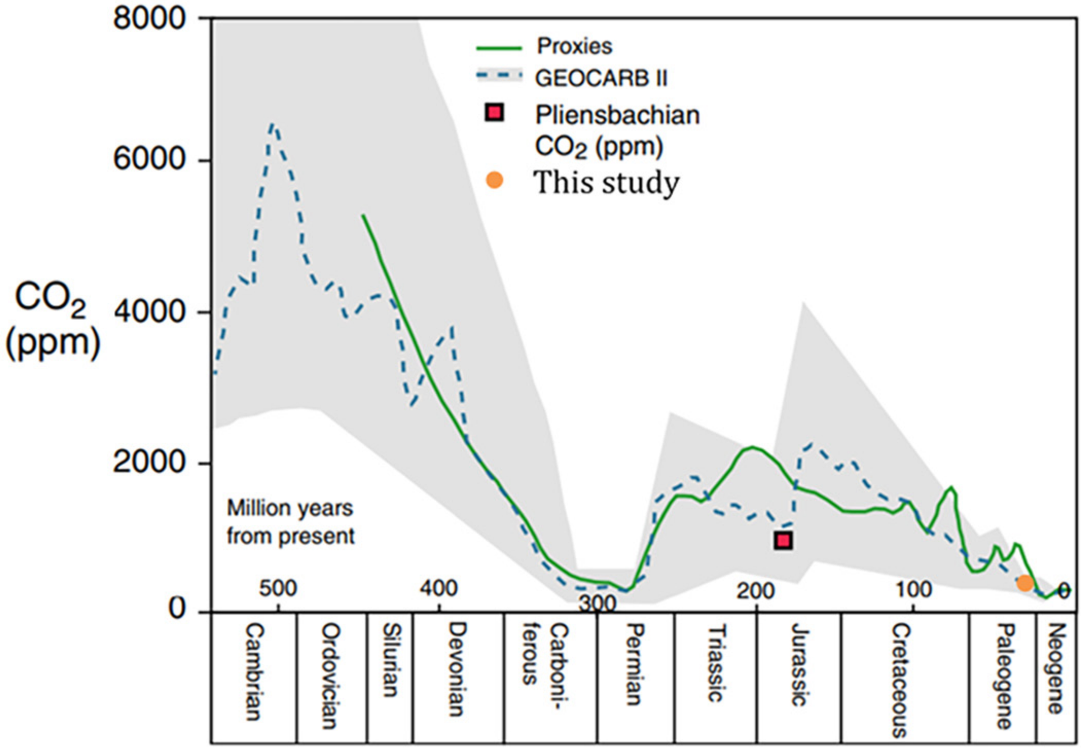

Fig. 5—Late Oligocene atmospheric CO_2 values shown by orange circle reconstructed using stomatal index and placed on the Phanerozoic atmospheric CO_2 reconstruction by Berner and Kothavala (2001), modified after Steinthorsdottir and Vajda, 2015.

et al., 2021). These values are in congruent with previous studies indicating that the late Oligocene is characterized by relatively low temperatures (Hansen *et al*., 2008; Zachos *et al*., 2008) and with the hypothesis that atmospheric CO_2 variations have contributed to this cold climate; estimates of atmospheric CO_2 from various climate proxies show similar low concentrations of CO_2 values for the late Oligocene compared to the preceding Eocene and the following Miocene Epochs (Berner & Kothavala, 2001; Grein *et al*., 2013; Steinthorsdottir & Vajda, 2015; Tesfamichael *et al*., 2017; O'Brien *et al*., 2020) (Fig. 5). Evidence for the relative cold climate during the late Oligocene comes from marine oxygen isotopes, biostratigraphic records, and ice volume estimates (Hansen *et al*., 2008; Zachos *et al*., 2008). Oxygen isotope studies of deep–sea sediments from the late Oligocene indicate a positive shift of $\delta^{18}O$ values, indicating increasingly cold surface waters (Zachos *et al*., 2008). Oxygen isotopes indicate lower temperatures than at any time earlier in the Cenozoic, other than at the Eocene–Oligocene boundary, or later into the early Miocene (Zachos *et al*., 2008; Pekar *et al*., 2006; Villa *et al*., 2008). The marine biostratigraphic record shows a sudden change in the composition of nannofossil assemblages during the late Oligocene (28.5 to 26.3 Ma), which also indicates cold surface–water conditions (Villa *et al*., 2008). A calibration of ^{18}O values to sea level by Pekar *et al*. (2006) for the late Oligocene shows a large accumulation of ice volume in the Antarctic and a corresponding reduction in sea level.

Although concentration of atmospheric CO_2 is the primary driver of stomatal–density variations, other variables such as humidity and light intensity (Poole *et al*., 1996) can influence the stomatal index of a leaf, and such factors can reduce the predictive strength of the calibrating curve by increasing the variance. Plants respond to variations of atmospheric CO_2 concentrations, and their upper ceiling response to CO_2 varies from plant to plant (Kouwenberg *et al*., 2003; Haworth *et al*., 2010); some plants have as high as 600 ppm such as Ginkgo biloba leaves and conifer species (Steinthorsdottir *et al*., 2022) and others have as low as 300 ppm such as Lauraceae (Kouwenberg *et al*, 2003; Berner, 2006; Steinthorsdottir *et al*., 2022). Hence ceiling response of plants for atmospheric CO_2 can influence the reconstructed CO_2 values. However, *Cynometra* species are tropical forest trees with a pantropical distribution, and they have originated and evolved in the hot tropical regions (Pan *et al*., 2010) similar to many of the plant species that have a higher ceiling response to atmospheric CO_2 variations. The quantified CO_2 values are at the end of the ceiling response range, and the effects of the ceiling response to the CO_2 values are minimal.

It is assumed that fossil leaves and their corresponding extant taxa behaved similarly and faced similar environmental and ecological conditions; if these conditions were different, they may increase the variance and in turn increase the margins of errors for the quantified CO_2 values.

The quantified atmospheric CO_2 values for the late Oligocene are vital as these fill a data gap in the geologic time slot and refine our understanding of earth's climate variations and improve resolution of climate models; these values are in congruent with the notion that concentration of atmospheric CO_2 played a significant role for the lower global temperatures during the late Oligocene.

Acknowledgements—*This work was supported by the Leakey Foundation: the Francis H. Brown African Scholarship Fund, Addis Ababa University and Southern Methodist University. The author thanks Addis Ababa University, Missouri Botanical Garden, and Botanical Research Institute of Texas for providing access to the herbarium collections. The author is grateful to the Authority for Research and Conservation of Cultural Heritage of Ethiopia for providing access to the laboratory facilities.*

REFERENCES

Ayalew D, Barbey P, Marty B, Reisberg L, Yirgu G & Pik R 2002. Source, genesis, and timing of giant ignimbrite deposits associated with Ethiopian continental flood basalts. Geochimica et Cosmochimica Acta 66: 1429–1448.

Berner RA 2006. GEOCARBSULF: a combined model for Phanerozoic atmospheric O_2 and CO_2. Geochimica et Cosmochimica Acta 70: 5653–5664.

Berner RA & Kothavala Z 2001. GEOCARB III: a revised model of atmospheric CO_2 over Phanerozoic time. American Journal of Science 301: 182–204.

Cotton LJ & Pearson PN 2011. Extinction of larger benthic foraminifera at the Eocene/Oligocene boundary. Palaeogeography, Palaeoclimatology, Palaeoecology 311: 281–296.

Coulie E, Quidelleur X, Gillot PY, Courtillot V, Lefèvre JC & Chiesa S 2003. Comparative K–Ar and Ar/Ar dating of Ethiopian and Yemenite Oligocene volcanism: implications for timing and duration of the Ethiopian traps. Earth and Planetary Science Letters 206: 477–492.

Escarguel G, Legendre S & Sigé B 2008. Unearthing deep–time biodiversity changes: The Palaeogene mammalian metacommunity of the Quercy and Limagne area (Massif Central, France). Comptes Rendus Geoscience 340: 602–614.

Franks PJ, Royer DL, Beerling DJ, Van de Water PK, Cantrill DJ, Barbour MM & Berry JA 2014. New constraints on atmospheric CO_2 concentration for the Phanerozoic. Geophysical Research Letters 41: 4685–4694.

Grein M, Oehm Ch, Konrad W, Utescher T, Kunzmann L & Roth–Nebelsick A 2013. Atmospheric CO_2 from the late Oligocene to early Miocene based on photosynthesis data and fossil leaf characteristics. Palaeogeography, Palaeoclimatology, Palaeoecology 374: 41–51.

Hansen J, Sato M, Kharecha P, Beerling D, Berner R, Masson–Delmotte V, Pagani M, Raymo M, Royer DL & Zachos JC 2008. Target Atmospheric CO_2: Where Should Humanity Aim?. The Open Atmospheric Science Journal 2: 217–231.

Haworth M, Heath J & McElwain JC 2010. Differences in the response sensitivity of stomatal index to atmospheric CO_2 among four genera of Cupressaceae conifers. Annals of Botany 105: 411–418.

Hodel F, Grespan R, Rafélis M, Dera G, Lezin C, Nardin E, Rouby D, Aretz M, Steinnman M, Buatier M, Lacan F, Jeandel C & Chavagnac C 2021. Drake Passage gateway opening and Antarctic Circumpolar Current onset 31 Ma ago: The message of foraminifera and reconsideration of the Neodymium isotope record. Chemical Geology 570: 120171.

Houben AJ, Mourik CA, Montanari A, Coccioni R & Brinkhuis H 2012. The Eocene–Oligocene transition: Changes in sea level, temperature or both? Palaeogeography, Palaeoclimatology, Palaeoecology 335–336: 75–83.

Hutchinson DK, Coxall HK, Lunt DJ, Steinthorsdottir M, Boer AM, Baatsen M, Heydt A, Huber M, Kennedy–Asser AT, Kunzmann L, Ladant J, Lear CH, Moraweck K, Pearson PN, Piga E, Pound MJ, Salzmann U, Scher HD, Sijp WP, Śliwińska KK, Wilson PA & Zhang Z 2020. The Eocene–Oligocene transition: a review of marine and terrestrial proxy data, models and model–data comparisons. Climate of the Past 68: 1–71.

Kappelman J, Rasmussen DT, Sanders WJ, Feseha M, Bown Th, Copeland P, Crabaugh J, Fleagle J, Glantz M, Gordon A, Jacobs B, Maga M, Muldoon K, Pan A, Pyne L, Richmond B, Ryan T, Seiffert ER, Sen S, Todd L, Wiemann MC & Winkler A 2003. Oligocene mammals from Ethiopia and faunal exchange between Afro–Arabia and Eurasia. Nature 426: 549–552.

Kieffer B, Arndt N, Lapierre H, Bastien F, Bosch D, Pecher A, Yirgu G, Ayalew D, Weis D, Jerram DA, Keller F & Meugniot C 2004. Flood and shield basalts from Ethiopia: magmas from the African superswell. Journal of Petrology 45: 793–834.

Konrad W, Royer DL, Franks PJ & Roth–Nebelsick A 2021. Quantitative critique of leaf–based paleo–CO_2 proxies: Consequences for their reliability and applicability. Geological Journal 56: 886–902.

Kouwenberg LR, McElwain JC, Kürschner WM, Wagner F, Beerling DJ, Mayle FE & Visscher H 2003. Stomatal frequency adjustment of four conifer species to historical changes in atmospheric CO_2. American Journal of Botany 90: 610–619.

Liu S, Feng Z, Lin H, Liu P, Liang M, Qing X, Xiong H, Qiu Sh, Li J, Jiang K, Hong H & Fang Sh 2021. Changes of atmospheric CO_2 in the Tibetan Plateau from 1994 to 2019. JGR Atmospheres 126: e2021JD035299.

McElwain JC & Haworth DM 2009. The stomatal–CO_2 proxy: limitations and advances. Geochimica et Cosmochimica Acta 73: A856.

Montañez IP & Poulsen CJ 2013. The late Paleozoic ice age: An evolving paradigm. Annual Review of Earth and Planetary Sciences 41: 629–656.

O'Brien ChL, Huber M, Thomas E, Pagani M, Super JR, Elder LE & Hull PM 2020. The enigma of Oligocene climate and global surface temperature evolution. PNAS 117: 25302–25309.

Pan AD, Jacobs BF & Herendeen PS 2010. Detarieae sensu lato (Fabaceae) from the Late Oligocene (27.23 Ma) Guang River flora of north–western Ethiopia. Botanical Journal of the Linnean Society 163: 44–54.

Pekar SF, DeConto RM & Harwood DM 2006. Resolving a late Oligocene conundrum: Deep–sea warming and Antarctic glaciation. Palaeogeography, Palaeoclimatology, Palaeoecology 231: 29–40.

Poole I, Weyers JB, Lawson T & Raven JA 1996. Variations in stomatal density and index: implications for palaeoclimatic reconstructions. Plant, Cell and Environment 19: 705–712.

Rasband WS 2016. ImageJ, U. S. National Institutes of Health, Bethesda, Maryland, USA: http://imagej.nih.gov/ij/.

Roth–Nebelsick A 2005. Reconstructing atmospheric carbon dioxide with stomata: possibilities and limitations of a botanical pCO_2–sensor. Trees 19: 251–265.

Royer DL 2001. Stomatal density and stomatal index as indicators of paleoatmospheric CO_2 concentration. Review of Palaeobotany and Palynology 114: 1–28.

Sen S 2013. Dispersal of African mammals in Eurasia during the Cenozoic: Ways and whys. Geobios 46: 159–172.

Shockey BJ & Anaya F 2011. Grazing in a New Late Oligocene Mylodontid Sloth and a Mylodontid Radiation as a Component of the Eocene–Oligocene Faunal Turnover and the Early Spread of Grasslands/Savannas in South America. Journal of Mammalian Evolution 18: 101–115.

Steinthorsdottir M, Jardine PE, Lomax BH & Sallstedt T 2022. Key traits of living fossil Ginkgo biloba are highly variable but not influenced by climate–Implications for palaeo–pCO_2 reconstructions and climate sensitivity. Global and Planetary Change 211: 103786.

Steinthorsdottir M & Vajda V 2015. Early Jurassic (late Pliensbachian) CO_2

concentrations based on stomatal analysis of fossil conifer leaves from eastern Australia. Gondwana Research 27: 932–939.

Sun J, Sheykh M, Ahmadi N, Cao M, Zhang Z, Tian Sh, Sha J, Jian Z, Windley BF & Talebian, M 2021. Permanent closure of the Tethyan Seaway in the northwestern Iranian Plateau driven by cyclic sea–level fluctuations in the late Middle Miocene. Palaeogeography, Palaeoclimatology, Palaeoecology 564: 110172.

Tesfamichael T, Jacobs B, Tabor N, Michel L, Currano E, Feseha M, Barclay R, Kappelman J & Schmitz M 2017. Settling the issue of "decoupling" between atmospheric carbon dioxide and global temperature: $[CO_2]_{atm}$ reconstructions across the warming Paleogene–Neogene divide. Geology 45: 999–1002.

Utescher T, Erdei B, François L, Henrot A, Mosbrugger V & Popova S 2020. Oligocene vegetation of Europe and western Asia–Diversity change and continental patterns reflected by plant functional types. Geological Journal 56: 628–649.

Villa G, Fioroni C, Pea L, Bohaty S & Persico D 2008. Middle Eocene–late Oligocene climate variability: Calcareous nannofossil response at Kerguelen Plateau, Site 748. Marine Micropaleontology 69: 173–192.

Vries D, Heritage S, Borths MR, Sallam HM & Seiffert ER 2021. Communications Biology 4: 1172.

Wang T, Li G, Aitchison JC & Sheng J 2020. Eocene ostracods from southern Tibet: Implications for the disappearance of Neo–Tethys. Palaeogeography, Palaeoclimatology, Palaeoecology 539: 109488.

Zachos JC, Dickens GR & Zeebe RE 2008. An early Cenozoic perspective on greenhouse warming and carbon–cycle dynamics. Nature 451: 279–283.